SOLID PARTICLE DISPERSION IN AGITATED TANKS BASED ON LES

Jos Derksen
Kramers Laboratorium voor Fysische Technologie
Delft University of Technology
Prins Bernhardlaan 6, 2628 BW Delft, The Netherlands
jos@klft.tn.tudelft.nl

ABSTRACT

Large-eddy simulations of the turbulent flow in a mixing tank have been coupled to a Lagrangian description of spherical, solid particles immersed in the flow. The working fluid was water, whereas the solid particles had the properties of glass beads. Simulations were restricted to a lab-scale tank (volume 10^{-2} m^3), and relatively low solids volume fractions (up to 3.6%). Two sets of particles were considered with particle diameter 0.30 mm and 0.47 mm respectively. It appeared to be essential to take particle-particle collisions into account, mainly because of their exclusion effect that prevents unrealistic build-up of particle concentrations closely above the bottom. The simulations give detailed insight in the behavior of the particles, and in the way the liquid flow is altered by the presence of the particles. The frequency and intensity of particle-particle collisions, and particle-impeller collisions have been investigated.

INTRODUCTION

Stirred tanks are true workhorses in the chemical and related industries. They are for instance used for blending, for promoting chemical reactions, for making liquid-liquid dispersions, and for gas-liquid contacting. Most of the applications rely on the turbulence generated by some sort of impeller (or combinations of multiple impellers) revolving in a baffled tank. An important class of applications involves particle dispersion, i.e. discrete solid particles suspended in a continuous liquid phase where particle motion is induced by, and sedimentation is prevented by the turbulent liquid flow. Such suspensions are encountered in industrial crystallization, in catalytic slurry reactors where the catalytic substance is carried by (porous) solid particles, and in particle coating processes for making pigments and paints.

There are many unresolved issues with respect to what is actually going on at the particle scale (in terms of e.g. heat and mass transfer, mechanical load on particles as a result of particle-particle and particle-impeller collisions) and how the presence of particles influences local and global flow features in the vessel such as the vortex structure in the vicinity of the impeller, power consumption, circulation and mixing times, and the distribution of turbulence quantities. Next to experiments, and theoretical considerations, numerical modeling is a way to investigate these issues.

Basis of the simulations discussed here is a representation of the continuous phase flow by means of large-eddy simulation (LES). This way of turbulence modeling leaves less room for speculation in modeling the turbulence and the motion of solids immersed in the flow compared to RANS-based turbulence modeling, at the expense of an increased computational effort. It has been clearly demonstrated that LES can accurately represent the single-phase flow in a stirred tank, including the turbulent fluctuation levels (Derksen and Van den Akker, 1999). In the LES flow field, spherical particles are released according to an Eulerian/Lagrangian (Eu/La) approach. We do not resolve the fluid-solid interface at the particle surface; the size of the particles is smaller than the LES grid-spacing. The dynamical behavior of the particles is determined by semi-empirical correlations for the forces exerted by a (inhomogeneous) fluid flow on single particles. The forces that are taken into account are gravity, drag, the force due to added mass, Saffman force, Magnus force, and the force due to stress gradients (pressure and viscous stress). Furthermore, particle-particle collisions and two-way coupling (i.e. the impact the presence of particles has on the continuous phase flow) are taken into account. Since in our Eu/La approach the hydrodynamic forces acting on the solid particles are based on correlations that are strictly speaking only valid for single particles in unbounded fluid flow, the volume fractions for which physically sound simulations can be done are limited. Furthermore, the computational effort spent on particle tracking is strongly dependent on the number of particles. These considerations forced us to limit the size of the tank, and the solids volume fractions applied here.

FLOW SYSTEM

The stirred tank has a standard configuration. It consists of a cylindrical, flat-bottomed, baffled tank with diameter (T) equal to the liquid height. The top of the vessel is closed with a lid. The impeller that drives the flow is a Rushton

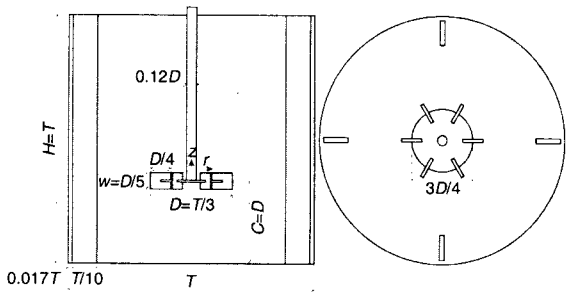

Figure 1. Flow geometry and (r,z) coordinate system. Left: side view, right: top view. The vessel content is covered with a lid (no-slip wall). The axial level with z=0 is at the impeller disk.

turbine with diameter $D=T/3$, placed with a bottom clearance $C=D$. The geometry is defined in Figure 1. The Reynolds number (that fully determines the single-phase flow) is defined as $Re=ND^2/\nu$, with N the impeller speed (in rev/s), and ν the kinematic viscosity of the working fluid.

In order to better appreciate the agitated solid-liquid system, we will now switch to dimensional numbers. The vessel volume was set to 10^{-2} m^3, which implies that D=7.78·10^{-2} m. The continuous phase was water (with ν=1·10^{-6} m^2/s, and ρ_l=1·10^3 kg/m^3). Two sets of particles were released in the tank. The first set (particle set #1) consisted of 6,705,623 spherical particles with diameter d_p=0.30 mm, and density ratio $\frac{\rho_p}{\rho_l}=2.5$ (with ρ_p the density of the particles), typical for glass beads in water. As a result, the solids volume and mass fractions amounted to Φ_V=0.95% and Φ_m=2.37% respectively. The impeller was set to revolve with N=16.5 rev/s (Re=1·10^5). The Stokes number of the particles was Stk=0.21 (with $Stk=\frac{\rho_p}{\rho_l}\frac{{d_p}^2 N}{18\nu}$). The impeller speed was chosen to be slightly above the just-suspended impeller speed N_{js} according to the empirical Zwietering (1958) correlation (see also Baldi et al., 1978) for this system: $N_{js}=s\frac{d_p^{0.2}\nu^{0.1}(|\mathbf{g}|\Delta\rho)^{0.45}\Phi_m^{0.13}}{\rho_l^{0.45}D^{0.85}}$=13 rev/s ($\mathbf{g}$ is the gravitational acceleration vector, $\Delta\rho=\rho_p-\rho_l$, and Φ_m is the solids mass fraction in %; the constant s=8 for our configuration). At and above N_{js}, the impeller runs sufficiently fast to have no solid matter resting at the bottom. As a consequence, the least requirement for the result of a simulation is that it indeed shows sufficient suspension of the solids.

The second set of particles (particle set #2) had d_p=0.468 mm. The number of particles and the density ratio were the same as for set #1. The solids volume fraction was now significantly higher: 3.6%. Also the just-suspended impeller speed increased for this system: N_{js}=17 rev/s. In the simulations with the second set of particles, the impeller speed was set to N=25 rev/s (Re=1.5·10^5; Stk=0.87).

MODELING ISSUES

Liquid Flow

For the single-phase (i.e. the Eulerian) part of the simulations, an in-house developed lattice-Boltzmann code has been employed. The features of the code that are relevant to turbulent, stirred tank flow have been documented in Derksen and Van den Akker (1999). In summary, lattice-Boltzmann methods provide a second-order discretization (in space and time) of the incompressible Navier-Stokes equation on a uniform, cubic lattice (Chen and Doolen, 1998). The method has been chosen for its flexibility with which complex flow geometries can be represented, and because of its parallel efficiency. The latter is due to the locality of its arithmetic operations, as a result of which parallelization based on domain decomposition only requires communication of limited amounts of subdomain-boundary data. This implies that parallel versions of the code run efficiently on cheap PC clusters (so-called Beowulf clusters).

The subgrid-scale model in the LES version of the code was the standard Smagorinsky model (Smagorinsky, 1963) with c_S=0.1. The grid consisted of 240^3 lattice cells, i.e. the grid-spacing amounted to approximately 1 mm.

Solid Particle Dynamics

For each particle, six dynamic equations are solved numerically: three for the linear, and three for the angular degrees of freedom. The equations of linear motion contain inertia, gravity, and hydrodynamic forces. From the linear velocities, the particle position is determined. The major hydrodynamic force on the particle is the drag force, with a drag coefficient that depends on the particle Reynolds number $Re_p=\frac{|\mathbf{u}-\mathbf{v_p}|d_p}{\nu}$ (with $\mathbf{v_p}$ and $\mathbf{u}$ the velocity of the particle, and the velocity of the liquid at the particle position respectively) according to $C_D=\frac{24}{Re_p}\left(1.0+0.15\,Re_p^{0.687}\right)$ for $Re_p<1{,}000$, and $C_D=0.44$ for $Re_p\geq 1{,}000$ (Sommerfeld, 2001). Furthermore, added mass, lift forces (Magnus force and Saffman force), and the force induced by stress gradients are taken into account. The lift forces have been calculated according to the non-Stokesian correlations due to Mei (1992), and Oesterlé and Bui Dinh (1998) that depend on the rotational Reynolds numbers $Re_S=\frac{|\boldsymbol{\omega}|{d_p}^2}{\nu}$, and $Re_R=\frac{\left|\frac{1}{2}\boldsymbol{\omega}-\boldsymbol{\omega}_\mathbf{p}\right|{d_p}^2}{\nu}$, with ω the vorticity of the fluid, and $\omega_\mathbf{p}$ the rotational velocity of the particle.

The determination of the Magnus force requires solving the equation of angular motion, which balances angular inertia,

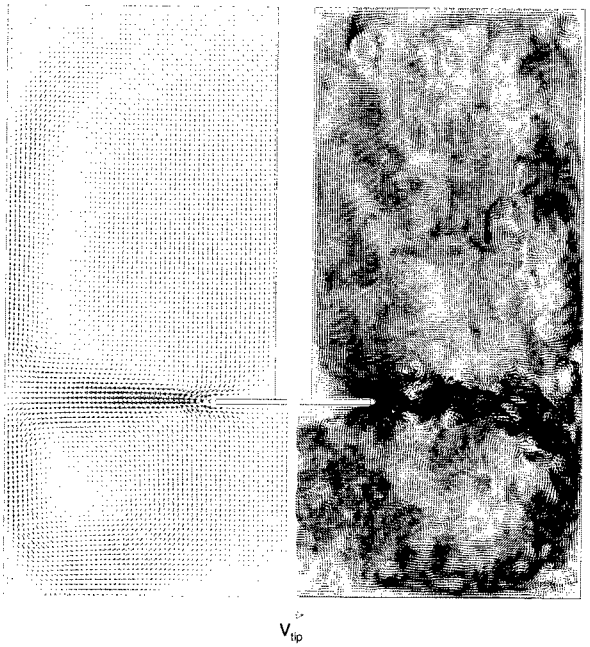

Figure 2. Velocity vector field at $Re=1\cdot10^5$ in the vertical plane, midway between two baffles. Left: time-averaged flow in half the spatial resolution; right: snapshot at the full resolution. One-way coupled simulation.

and viscous damping. The particles' angular velocity may also be relevant for liquid-solid mass transfer.

The fluid's velocity, vorticity, pressure, and viscous stress contained in the equations of motion all consist of a resolved and a subgrid-scale part. For reasons of simplicity, the subgrid-scale parts have been discarded, except when the drag force is involved. For determining the drag force, the local fluid velocity is considered to be the sum of the resolved velocity and a Gaussian random process with standard deviation $u_{sgs}=\sqrt{\frac{2}{3}k_{sgs}}$ representing the subgrid-scale motion. The subgrid-scale kinetic energy k_{sgs} was estimated based on isotropic, local-equilibrium mixing-length reasoning (Mason and Callen, 1986).

Three types of collisions need to be distinguished: particle-wall, particle-impeller, and particle-particle collisions. Collisions of all types were considered to be fully elastic and frictionless (the latter implies that in a particle-wall and particle-impeller collision the wall parallel components of the velocity of the particle *surface* are unchanged after a collision; in a particle-particle collision the rotation of the particles does not play a role in the collisional process). For the particle-impeller collisions, only a collision with one of the (six) impeller blades adds momentum to a particle since only the impeller blades have a velocity component in their wall-normal direction.

The method for detecting and handling particle-particle collisions was similar to the one proposed by Chen et al. (1998). They make use of a collision detection algorithm that anticipates collisions in the upcoming time step. Subsequently, the path of two particles that are bound to collide is integrated in a three-step-process: the pre-collision step, the collision step (in which the particles exchange momentum), and the post-collision step. The collision algorithm assumes that one particle can only collide once during one time step. The reason is purely practical: taking into account multiple collisions in one time step would lengthen the computations to an unfeasible extent.

In the simulations, solids volume fractions are such that it is expected that two-way coupling effects are relevant (Elgobashi, 1994). Two-way coupling was achieved by feeding the force that the fluid exerts on a particle back to the fluid.

RESULTS

Impressions

Overall impressions of the flow field, and the distribution of particles are given in Figures 2 and 3 respectively. In Figure 2, an instantaneous realization of the flow in the vertical plane midway between two baffles is compared to the time-averaged flow. This figure illustrates the relevance of performing time-dependent flow simulations with a view to particle tracking. For a particle released in the tank, the average flow is an artifact:

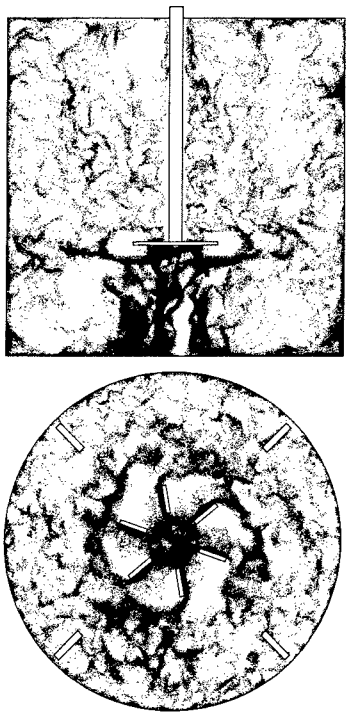

Figure 3. Instantaneous realization of the particle distribution in the tank for particle set #2. Top: vertical cross section through the center of the tank midway between two baffles; bottom: horizontal cross section at z/T=0.308 (i.e. just below the impeller disk). The impeller rotates in the counter-clockwise direction.

the particle will feel the eddy-like, erratic structures in the instantaneous flow field, not the smooth average field. Furthermore, heat and mass-transfer between solid and liquid is likely to be dominated by the fluctuations, rather than by the average flow.

The single realization of the particle distribution in two cross-sections in the tank (Figure 3) shows some peculiar features. In the horizontal cross section, large voids behind, and high solids concentrations in front of the blades are observed. As a result, high particle-impeller collision frequencies can be anticipated. The streaks of particles that are shed from the blades keep their identity over quite a radial distance and give rise to high time-average particle concentrations at the impeller level outside the impeller swept volume. Centrifugal forces induce high solids concentrations in the vicinity of the tank's outer wall. The vertical section shows particles throughout the tank, organized in streaky patterns. The concentrations are high at the bottom and outer wall. The upwardly flowing region underneath the impeller carries highly concentrated slurry towards the impeller. The region void of particles extending from the bottom to closely underneath the impeller slightly left from the tank's centerline is the manifestation of a slowly precessing vortex that (at the moment the snapshot was taken) crossed the vertical cross section. The locally high vorticity inhibits the presence of particles. The precessing vortex is a manifestation of a macro-instability in the stirred tank (Nikiforaki et al., 2002).

Two-way Coupling Effects

The presence of solid particles alters the turbulent flow field in the tank. The strongest influence of the particles is felt in the impeller stream: here the slip velocities are highest due to vigorous turbulent motion on the one hand and particle inertia on the other. The ratio between the particle relaxation time and the time between two blade passages equals six times (there are six impeller blades) the Stokes number. For the two particle sets considered here, this ratio is of the order of unity, and as a result the particles are given insufficient time to relax to the local flow field before another impeller blade passes by. The high slip velocities induce appreciable momentum exchange between solid and liquid, which alters the local flow field.

Figure 4 displays the time-averaged impeller outstream profiles for one-way, and two-way coupled cases of the tangential, and radial velocity, as well as of the turbulent kinetic energy $k = \frac{1}{2}\left(\overline{\langle u_i^2\rangle_\theta - \langle u_i\rangle_\theta^2}\right)$, where the brackets $\langle\ \rangle_\theta$ indicate conditional averages at impeller position θ, and the overbar indicates averaging over all angular positions (the subscript i denotes the velocity components, and the summation convention has been applied). Especially the impact of the particles on the k-levels close to the impeller is considerable: turbulence appears to be damped by the particles. At $2r/D$=1.2 and $2r/D$=1.5, the particles make the k-profile much more asymmetric with respect to the impeller disk level. The

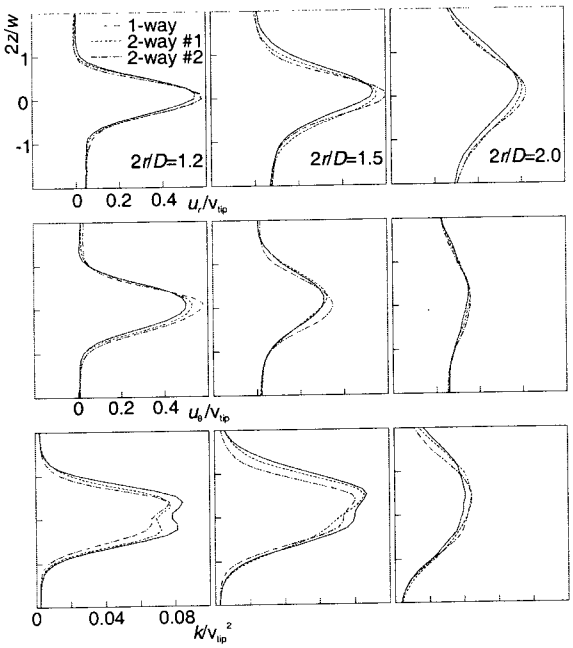

Figure 4. Time-averaged impeller outstream profiles in the plane midway between two baffles at (from left to right) three radial positions. Comparison between 1-way coupled, and 2-way coupled simulations with particle sets #1 and #2. From top to bottom: radial velocity, tangential velocity, and turbulent kinetic energy.

asymmetry is due to the particle concentration being much higher underneath the disk than above the disk. The maximum tangential and radial time-average velocity in the

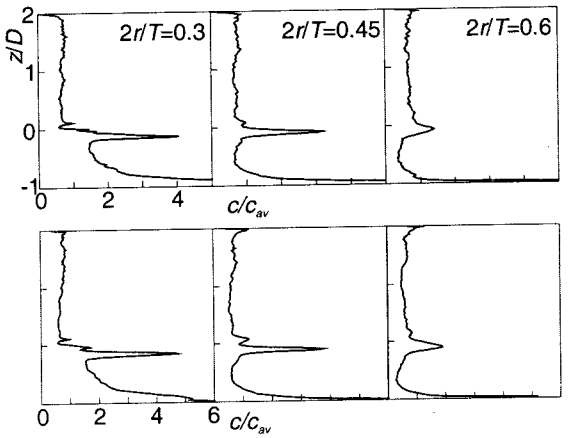

Figure 5. Time-averaged particle concentration in the plane midway between two baffles as a function of the vertical position in the tank at three different radial positions. Comparison between particle set #1 (top), and set #2 (bottom). Note the different concentration scales in the top and bottom graphs.

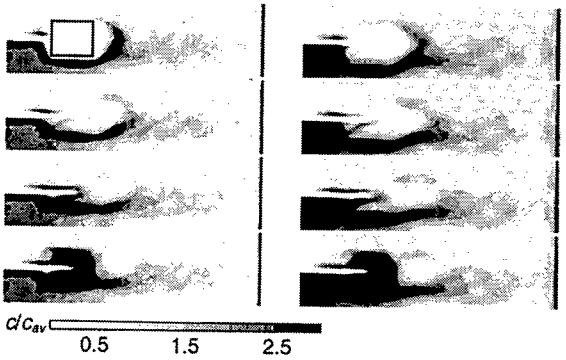

Figure 6. Conditionally averaged (at specific angular positions of the impeller) particle concentration fields in a vertical plane midway between two baffles in the vicinity of the impeller (for reference, the zero-angle blade position has been indicated in the upper left graph). Left: particle set #1; right: particle set #2. From top to bottom: 15°, 30°, 45°, and 55° behind the impeller blade.

vicinity of the impeller tip is increased in the presence of particles due to particle inertia. At radial positions further away from the impeller (at $2r/D$=2.0), all profiles more or less relax to the single-phase (i.e. one-way coupled) profiles.

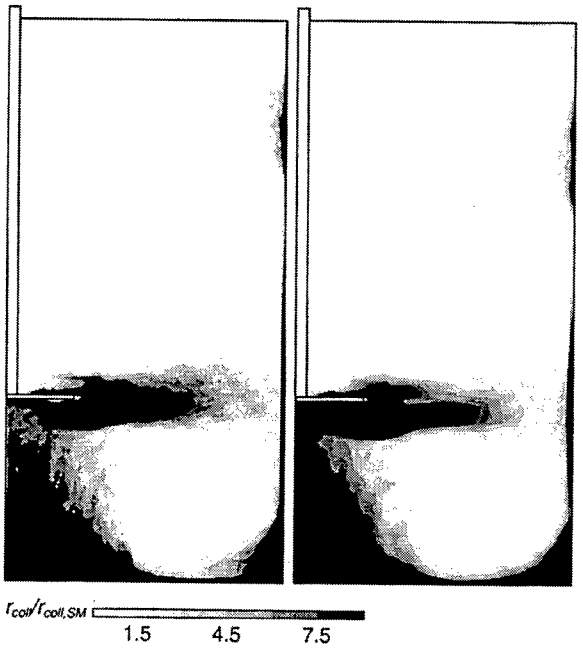

Figure 7. Time-averaged contours of the particle-particle collision rate in the vertical plane midway between two baffles. Left: particle set #1; right: particle set #2. The collision rate has been normalized with the Von Smulochowski collision rate $r_{coll,Sm}$ (Eq. 1).

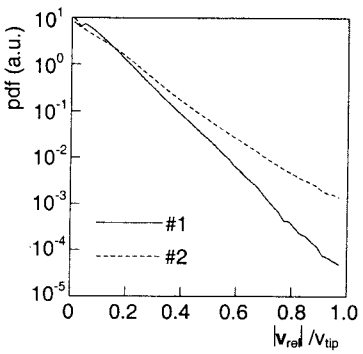

Figure 8. Probability density function of the relative velocity at particle-impeller-blade impact. Comparison of particle set #1 and #2.

Particle Concentration Fields

The observations related to Figure 3 are reflected in the time-averaged, axial particle number concentration profiles in Figure 5: high concentrations closely above the bottom, and at the level of the impeller. The latter peak-concentration is due to the accumulation of particles in front of the impeller blades. For the bigger particles (set #2), the peak is more pronounced. Above the impeller, the concentration of particles is almost uniform with $c \approx 0.7 c_{av}$ for both particle sets.

The way the particles interact with the blades has been depicted in Figure 6. It shows a quantitative view of the regions void of particles in the wake of the impeller blades, and the accumulation of particles in front of the blades (the 55° position). The void is advected radially into the bulk of the tank at a pace similar to the upper trailing vortex that develops in the wake of the impeller blade.

Collisions

In this section, two types of collisions will be considered: particle-particle and particle-impeller collisions. Collisions in turbulently agitated solid-liquid systems are highly relevant. Particle breakage is considered to be the result of particles colliding with one another, or with the internals of the reactor. In industrial crystallization, breakage of particles is a main source of secondary nucleation, and therefore strongly influences product quality. In catalytic slurry reactors, wear of the solids is a significant problem, since it degrades the catalytic material and makes separation steps (fines removal) necessary.

In order to usefully compare the simulations with the two particle sets, we non-dimensionalized the observed collision rate with the collision rate from the Von Smulochowski (1917) relation for particle collisions in shear flow:

$$r_{coll,Sm} = \frac{4}{3}\dot{\gamma} d_p^3 c_{av}^2 \qquad (1)$$

For the shear rate $\dot{\gamma}$, a tank-average value based on the tank-average dissipation rate $\bar{\varepsilon}$ has been applied: $\dot{\gamma} = \sqrt{\frac{\bar{\varepsilon}}{\nu}}$. The

tank average dissipation rate amounts to $\bar{\varepsilon} = \frac{Po N^3 D^5}{V_{tank}}$ with Po=5.0 the power number for a Rushton turbine revolving in a baffled tank (Rushton et al., 1950), and V_{tank} the volume of the tank. In time-averaged terms, the results are in Figure 7. The two contour plots look quite similar, demonstrating that the normalization with the Von Smulochowski relation is a fair way to scale the system in terms of collision rates. Since Eq. 1 contains the particle size d_p to the power three, whereas the average dissipation rates scales like $\bar{\varepsilon} \propto N^3$, in absolute terms the collision rate for particle set #2 is typically seven times the rate encountered with particle set #1. The relative velocities at particle-particle impact are highest in the impeller swept volume, and in the impeller stream (not shown).

Results on particle-impeller collisions are sown in terms of the *pdf* of the relative velocity at impact. This *pdf* has an exponential shape, see Figure 8. Increasing the size of the particles leads to a significantly higher chance on high-velocity particle-impeller collisions.

For the flow systems defined here, particle-particle collisions are much more frequent than particle-impeller collisions. With set #1, a particle collides on average 0.11 times per impeller revolution with the impeller, and 5.1 times with another particle; with set #2 these numbers are 0.21, and 14.1 respectively. The intensity of the particle-particle, and particle-impeller collisions (in terms of the relative velocity at impact) is quite comparable.

CONCLUSIONS

Two-phase (solid-liquid) simulations of the turbulent flow in a mixing tank according to an Eulerian/Lagrangian approach have been presented. In this approach, a large number (6.7 million) of particles was tracked in a liquid flow field that was represented by a large-eddy simulation (LES).

The simulations show some typical features with respect to the distribution of solids in the tank. The particles organize in streaky patterns, thereby avoiding high-vorticity regions. The region underneath the Rushton turbine carries highly concentrated slurry towards the impeller. In front of the impeller blades, particles accumulate; behind the impeller blades, large volumes void of particles are formed. The net effect is a peak in the time-averaged particle concentration at the axial level of the impeller.

The simulations gave detailed, quantitative insight in the particle behavior in the tank: time-averaged, and conditionally averaged (with the impeller angle) particle concentration fields, linear and rotational slip velocities, and data on collisions. The intensity of particle-particle, and particle-impeller collisions (in terms of the relative velocity at impact) proved to be quite comparable. For the specific flow systems studied in this article, however, the number of particle-particle collisions was much higher than the number of particle-impeller collisions.

ACKNOWLEDGEMENT

The author acknowledges support by the EU under the Growth Programme project Optimization of Industrial Multiphase Mixing (G1RD-CT-2000-00263).

REFERENCES

Baldi, G., Conti, R., and Alaria, E., 1978, "Complete suspension of particles in mechanically agitated vessels", *Chemical Engineering Science*, Vol. 33, pp. 21-25.

Chen, M., Kontomaris, K., and McLaughlin, J.B., 1998, "Direct numerical simulation of droplet collisions in a turbulent channel flow. Part I: collision algorithm", *International Journal of Multiphase Flow*, Vol. 24, pp. 1079-1103.

Chen, S., and Doolen, G.D., 1998, "Lattice Boltzmann method for fluid flows", *Annual Review Fluid Mechanics*, Vol. 30, 329-364.

Derksen, J.J., and Van den Akker, H.E.A., 1999, "Large eddy simulations on the flow driven by a Rushton turbine", *AIChE Journal*, Vol. 45, 209-221.

Elgobashi, S., 1994, "On predicting particle-laden turbulent flows", *Applied Scientific Research*, Vol. 52, pp. 309-329.

Mason, P.J., and Callen, N.S., 1986, "On the magnitude of the subgrid-scale eddy coefficient in large-eddy simulations of turbulent channel flow", *Journal of Fluid Mechanics*, Vol. 162, pp. 439-462.

Mei, R., 1992, "An approximate expression for the shear lift force on a spherical particle at finite Reynolds numbers", *International Journal of Multiphase Flow*, Vol. 18, pp. 145-147.

Nikiforaki, L., Montante, G., Lee, K.C., and Yianneskis, M., 2002, "On the origin, frequency and magnitude of macro-instabilities of the flows in stirred vessels", Submitted to *Chemical Engineering Science*.

Oesterlé, B, and Bui Dinh, T., 1998, "Experiments on the lift of a spinning sphere in the range of intermediate Reynolds numbers," *Experiments in Fluids*, Vol. 25, pp. 16-22.

Rushton, J.H., Costich, E.W., and Everett, H.J., 1950, "Power characteristics of mixing impeller I and II", *Chemical Engineering Progress*, Vol. 46, pp. 395-404 and 467-476.

Smagorinsky, J., 1963, "General circulation experiments with the primitive equations: 1. The basic experiment", *Monthly Weather Review*, Vol. 91, pp. 99-164.

Sommerfeld, M., 2001, "Validation of a stochastic Lagrangian modelling approach for inter-particle collisions in homogeneous isotropic turbulence", *International Journal of Multiphase Flow*, Vol. 27, pp. 1829-1858.

Von Smulochowski, M., 1917, "Versuch einer mathemischen Theorie der Koagulationkinetik kolloider Lösungen", *Zeitschrift für Physikalische Chemie*, Vol. 92, pp. 129-168.

Zwietering, Th.N., 1958, "Suspending of solid particles in liquid by agitators," *Chemical Engineering Science*, Vol. 8, 244-253.